Biol. Cybern. 85, 51–64 (2001)

Biological Cybernetics

Complex nonlinear dynamics of the Hodgkin–Huxley equations induced by time scale changes

Shinji Doi, Shuhei Nabetani, Sadatoshi Kumagai

Department of Electrical Engineering, Graduate School of Engineering, Osaka University, 2-1 Yamadaoka, Suita, Osaka 565-0871, Japan

Received: 9 August 2000 / Accepted in revised form: 10 January 2001

Abstract. The Hodgkin–Huxley equations with a slight modification are investigated, in which the inactivation process (h) of sodium channels or the activation process of potassium channels (n) is slowed down. We show that the equations produce a variety of action potential waveforms ranging from a plateau potential, such as in heart muscle cells, to chaotic bursting firings. When h is slowed down – differently from the case of n variable being slow – chaotic bursting oscillations are observed for a wide range of parameter values although both variables cause a decrease in the membrane potential. The underlying nonlinear dynamics of various action potentials are analyzed using bifurcation theory and a so-called slow–fast decomposition analysis. It is shown that a simple topological property of the equilibrium curves of slow and fast subsystems is essential to the production of chaotic oscillations, and this is the cause of the large difference in global firing characteristics between the h-slow and n-slow cases.

1 Introduction

Neurons and many other cells mainly utilize electrical signals to transfer information in nervous systems such as the brain and to control biological organs such as the heart. Neurons produce an action potential which is a rapid increase then decrease of the membrane voltage in response to external stimuli. Action potentials are the main information carrier in nervous systems, and the waveform (and thus the underlying nonlinear dynamics) of action potentials differ considerably from cell to cell (Hille 1992).

The famous Hodgkin–Huxley (HH) equations (Hodgkin and Huxley 1952) are a model of a squid giant axon that describes the generation of an action potential quantitatively (but see Strassberg and DeFelice 1993; Clay 1998). The equations are important not only as one of the most successful mathematical models in quantitatively describing biological phenomena, but also in that the method (HH formalism) used in deriving the model of a squid is directly applicable to many kinds of neurons and other cells. The equations derived following this HH formalism are called HH-type equations.

Following the HH formalism, various kinds of HH-type equations have been proposed (Chay and Keizer 1983; Cronin 1987; Rinzel 1990; Canavier et al. 1991; Traub et al. 1991; Noble 1995; Keener and Sneyd 1998). HH-type equations include many variables depending on the number of different ionic currents and their gating variables, whereas the original HH equations possess only four variables (membrane voltage, activation and inactivation variables of the Na^+ current, and an activation variable of the K^+ current). These HH-type equations can reproduce the action potentials of real neurons quantitatively and thus can be considered as a virtual neuron. Therefore, it is important to analyze the HH-type equations and to clarify the generation mechanism of action potentials.

So far, the original HH equations (Plant 1976; Rinzel 1978; Hassard 1978; Troy 1978; Rinzel and Miller 1980; Bedrov et al. 1992; Guckenheimer and Labouriau 1993; Fukai et al. 2000a,b) and various kinds of HH-type equations (Chay and Rinzel 1985; Alexander and Cai 1991; Canavier et al. 1993; Av-Ron 1994; Bertram 1994; Rush and Rinzel 1995; Schweighofer et al. 1999) have been analyzed numerically and/or analytically. The importance of differing time scales has already been demonstrated in the production of bursting oscillations in many types of cells. However, the essential factor in producing specific membrane potential waveforms is not clear, since many factors (the number of variables, functional forms of nonlinear functions, and constants) differ considerably from model to model.

The main purpose of the present article is to provide a viewpoint that unifies the previous studies on specific HH-type models, and to clarify the diversity and common features in the nonlinear dynamics of diverse

Correspondence to: S. Doi
(e-mail: doi@pwr.eng.osaka-u.ac.jp)

HH-type equations. To do so, as a first step, we consider the original HH equations of a squid which is the simplest HH-type model. As a prototypical model, we propose modified HH equations whose time constants are the only modification from the original ones. Despite this small change, it is shown that the equations can reproduce the various action potential waveforms of diverse neurons, and exhibit signal transmission properties that are completely different from the original ones. By a numerical bifurcation analysis using the AUTO software package (Doedel et al. 1995) and a so-called slow–fast analysis (Rinzel and Lee 1986), the generation mechanism underlying a variety of action potentials in the modified HH equations is explored. In particular, we investigate why chaotic bursting oscillations appear over a wide range of parameter values when the inactivation process (h) of the Na^+ current is slowed but not when the activation process (n) of the K^+ current is slowed.

2 Bifurcation analysis of the HH equations

Consider the following modified HH equations for a space-clamped squid giant axon:

$$\frac{dv}{dt} = G(v,m,n,h) + I_{\text{ext}} \tag{1a}$$

$$\frac{dm}{dt} = \frac{1}{\bar{\tau}_m \tau_m(v)}(m^\infty(v) - m) \tag{1b}$$

$$\frac{dn}{dt} = \frac{1}{\bar{\tau}_n \tau_n(v)}(n^\infty(v) - n) \tag{1c}$$

$$\frac{dh}{dt} = \frac{1}{\bar{\tau}_h \tau_h(v)}(h^\infty(v) - h) \tag{1d}$$

$$\begin{aligned} &G(v,m,n,h) \\ &\quad = I_{\text{Na}}(v,m,h) + I_{\text{K}}(v,n) + I_{\text{L}}(v) \\ &\quad = \bar{g}_{\text{Na}} m^3 h(V_{\text{Na}} - v) + \bar{g}_{\text{K}} n^4 (V_{\text{K}} - v) + \bar{g}_{\text{L}}(V_{\text{L}} - v) \end{aligned}$$

$$\bar{g}_{\text{Na}} = 120, \quad \bar{g}_{\text{K}} = 36, \quad \bar{g}_{\text{L}} = 0.3, \quad V_{\text{Na}} = 115,$$
$$V_{\text{K}} = -12, \quad V_{\text{L}} = 10.599$$

$$\tau_x(v) = \frac{1}{\alpha_x(v) + \beta_x(v)},$$
$$x^\infty(v) = \frac{\alpha_x(v)}{\alpha_x(v) + \beta_x(v)}, \quad x = m,n,h$$

$$\alpha_m(v) = \frac{0.1(25 - v)}{\exp[(25 - v)/10] - 1}, \quad \beta_m(v) = 4e^{-v/18}$$
$$\alpha_n(v) = \frac{0.01(10 - v)}{\exp[(10 - v)/10] - 1}, \quad \beta_n(v) = 0.125e^{-v/80}$$
$$\alpha_h(v) = 0.07\exp[-v/20], \quad \beta_h(v) = \frac{1}{\exp[(30 - v)/10] + 1}$$

where v is the membrane potential, and m, n, h are the gating variables: m and h are the activation and inactivation variables of the Na^+ ionic channel, respectively, and n is the activation variable of the K^+ channel. I_{ext} is the constant current that is externally applied to a neuron. Note that in these equations the membrane potential has been shifted in a depolarized direction so that the resting potential becomes zero when $I_{\text{ext}} = 0$.

The only modification from the original HH equations is the introduction of the 'time constants' $\bar{\tau}_m$, $\bar{\tau}_n$, and $\bar{\tau}_h$; in the case of $\bar{\tau}_m = \bar{\tau}_n = \bar{\tau}_h = 1$, these equations are equal to the original HH equations. In the following, the modified HH equations are also called the HH equations except where any confusion is possible.

Throughout the present article we consider the dependence of the HH equations' behavior on the parameter I_{ext}; we investigate the constant-current transfer characteristics of the HH neuron since they are considered to be the basis of the neuronal information transduction characteristics to more complicated synaptic inputs such as periodic pulsatile stimuli (Doi and Sato 1995; Doi et al. 1999).

Figure 1 shows examples of waveforms of the membrane potential v of the HH equations (1) when n is slow ($\bar{\tau}_n = 100$), while Fig. 2 corresponds to the case that h is slow ($\bar{\tau}_h = 100$). It can be seen that the shape of the membrane potential varies with the external constant current I_{ext}.

Figure 3 is the bifurcation diagram of the HH equations (1) for the bifurcation parameter I_{ext}; the (local) extrema of the membrane potential $v(t)$ after the transient dies are plotted for each value of I_{ext}. Figure 3a is the case in which n is the slow variable and Fig. 3b is the case in which h is the slow variable. Both bifurcation diagrams are completely different from that of the original HH equations, in which only a simple oscillation appears (see Fig. 4). We note that in contrast to Fig. 3a, in Fig. 3b various chaotic oscillation are observed over a wide range of values of the external current I_{ext}.

These (one-parameter) bifurcation diagrams are calculated by numerical simulations. Thus they show only stable solutions and are not bifurcation diagrams in a rigorous sense because 'bifurcation analysis' is not actually performed (i.e., they are only brute-force simulations with various values of the parameter I_{ext}). So, first of all, we made detailed bifurcation analyses of the (modified) HH equations (1) using the AUTO software package (Doedel et al. 1995).

2.1 One-parameter bifurcation analysis

First let us show the bifurcation diagram of the original HH equations (1) ($\bar{\tau}_m = \bar{\tau}_n = \bar{\tau}_h$), even though such an analysis has already been performed by many researchers (Rinzel 1978; Guttman et al. 1980; Rinzel and Miller 1980). Figure 4 shows such bifurcation diagrams; the v values of the stationary solution of the HH equations

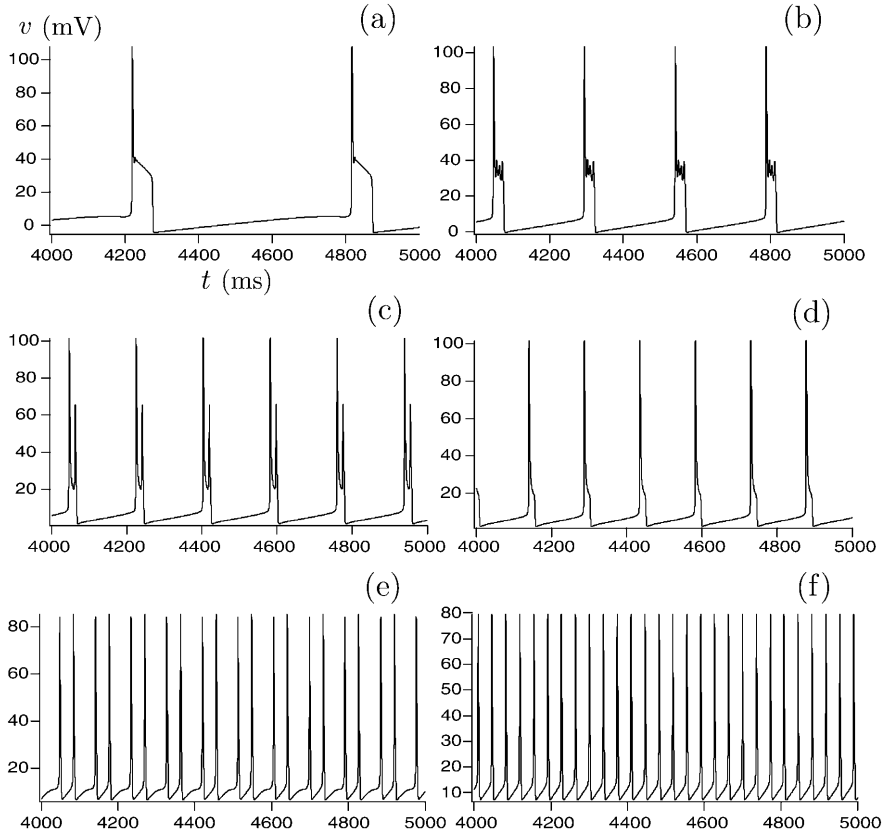

Fig. 1. Examples of waveforms of the membrane potential $v(t)$ of the HH equations (1) when n is slow ($\bar{\tau}_n = 100$). The value of I_{ext} is: **a** 10.0, **b** 20.0, **c** 24.2571, **d** 24.2572, **e** 60.0, and **f** 70.0

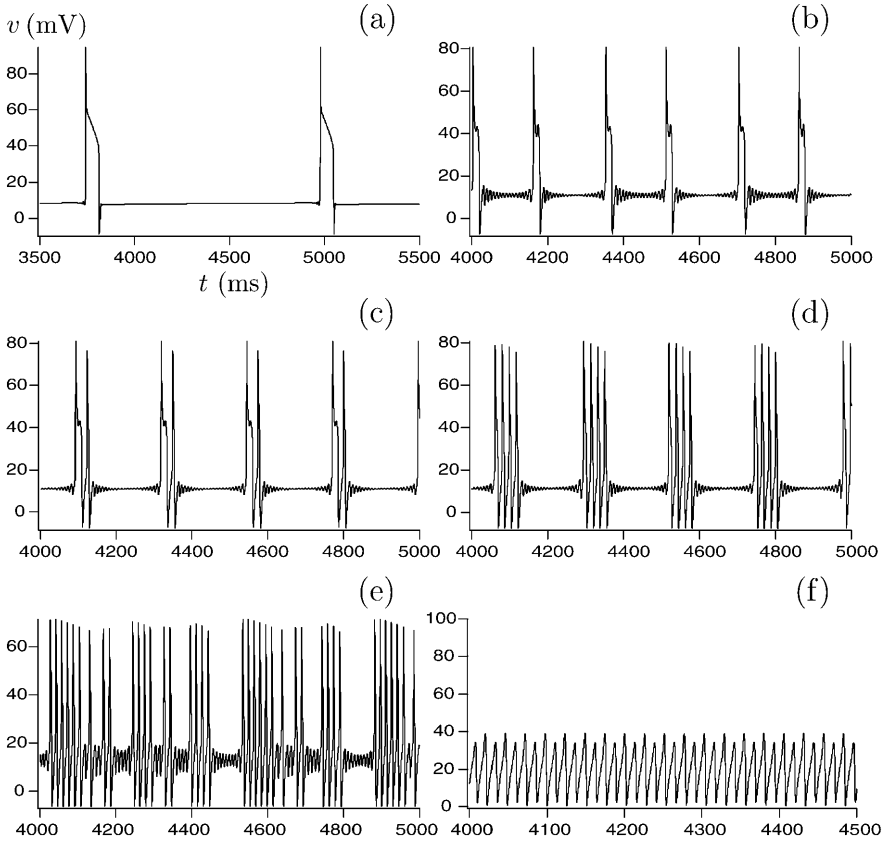

Fig. 2. Examples of waveforms of the membrane potential $v(t)$ of the HH equations (1) when h is slow ($\bar{\tau}_h = 100$). The value of I_{ext}: **a** 20.0, **b** 36.0, **c** 36.5, **d** 38.0, **e** 50.0, and **f** 91.0

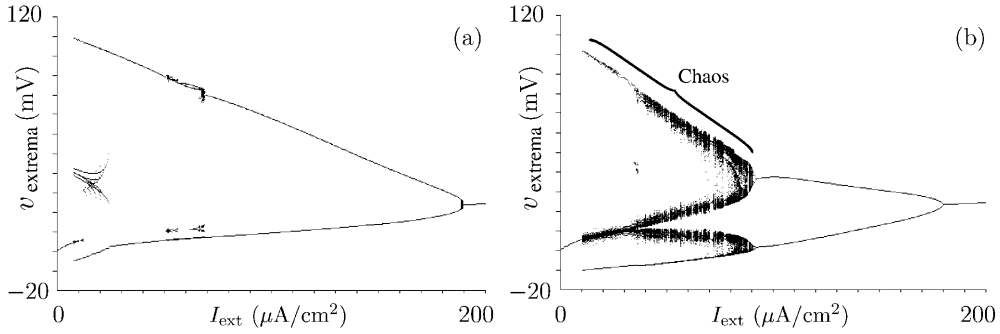

Fig. 3. Bifurcation diagram of the HH equations (1) when the bifurcation parameter is the external constant current I_{ext}. Local extrema of membrane potential $v(t)$ are plotted for each value of I_{ext}. **a** The n-slow case ($\bar{\tau}_n = 100$, $\bar{\tau}_m = \bar{\tau}_h = 1$). **b** The h-slow case ($\bar{\tau}_h = 100$, $\bar{\tau}_m = \bar{\tau}_n = 1$)

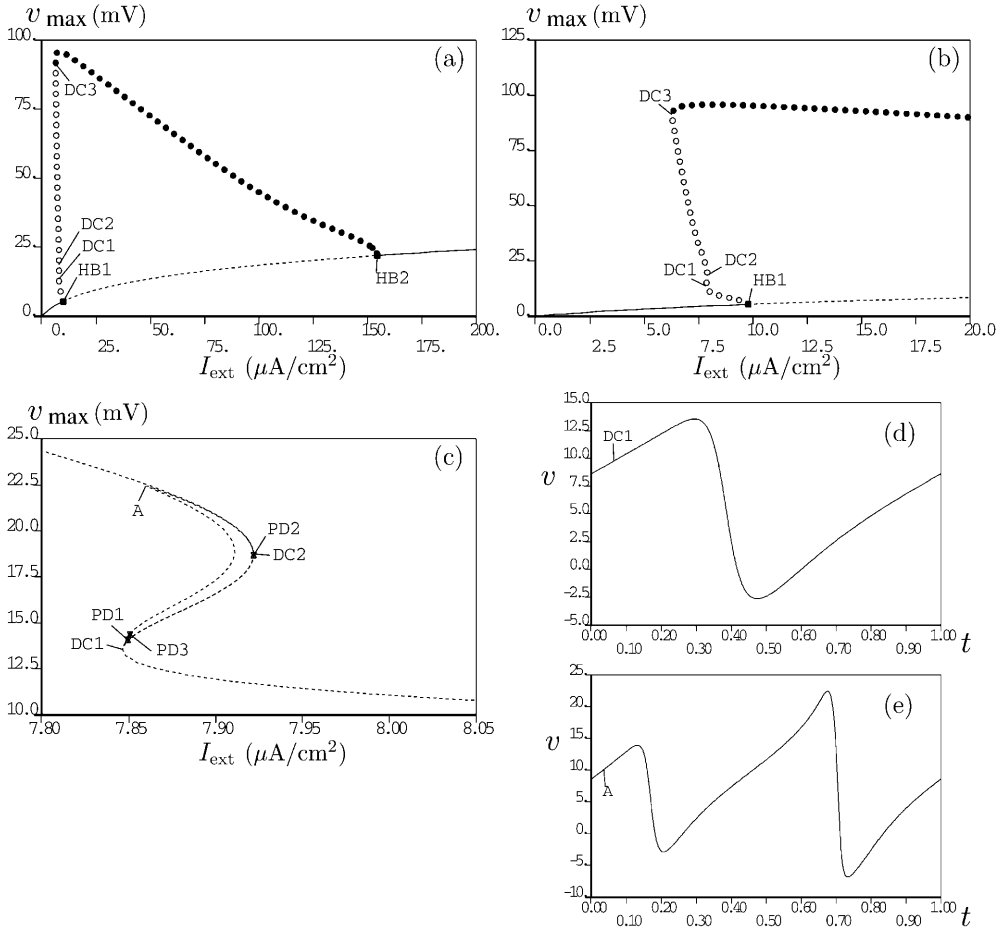

Fig. 4. **a** One-parameter *bifurcation diagram* of the original HH equations. Maximal values of the membrane potential of stable (*solid line*) or unstable (*dotted line*) equilibria and stable (*filled circles*) and unstable (*open circles*) periodic orbits are plotted for each value of I_{ext}. *HB* and *DC* denote the Hopf and double-cycle (saddle-node of periodic orbits) bifurcation points, respectively. **b** Magnification of **a**. **c** Magnification of **b** (*PD* denotes period-doubling). **d** Membrane potential waveform at point DC1 of **c**. **e** Membrane potential waveform at point A of **c**. Abscissa is the time normalized by its period

are plotted for various values of I_{ext}, while the maximum value of v is plotted for a periodic (oscillatory) solution – differently from Fig. 3. Solid and dotted lines denote stable and unstable equilibria, respectively. The filled (open) circles denote stable (unstable, resp.) periodic solutions. Figure 4b is the magnification of left part of Fig. 4a, and we can verify the multiple stability of an equilibrium and a periodic solution in the range of $6.3 < I_{ext} < 9.8$.

At point HB2 in Fig. 4a, a stable periodic solution bifurcates from an equilibrium point by the (supercritical or stable) Hopf bifurcation. An unstable periodic solution is bifurcated by the (subcritical or unstable) Hopf bifurcation at point HB1. As is seen from Fig. 4b, a multistability occurs near a subcritical Hopf bifurcation. At point DC3, a double-cycle bifurcation or a saddle-node bifurcation of periodic orbits occurs, and a pair of stable and unstable periodic solutions is generated. At both points DC1 and DC2, double-cycle bifurcations also occur. Figure 4c is the magnification of the region near points DC1 and DC2 of Fig. 4b where, for the sake of clarity, dotted curves are used to denote unstable periodic solutions rather than open circles. At point PD1, a period-doubling bifurcation of an unstable periodic solution occurs, and a branch of unstable periodic orbits with 'double period' is bifurcated. This bifurcated branch turns over at point A and ends at an another period-doubling bifurcation point PD2. Thus, near $I_{ext} = 7.9$, seven periodic solutions (one stable solution and six unstable solutions) coexist (Rinzel and

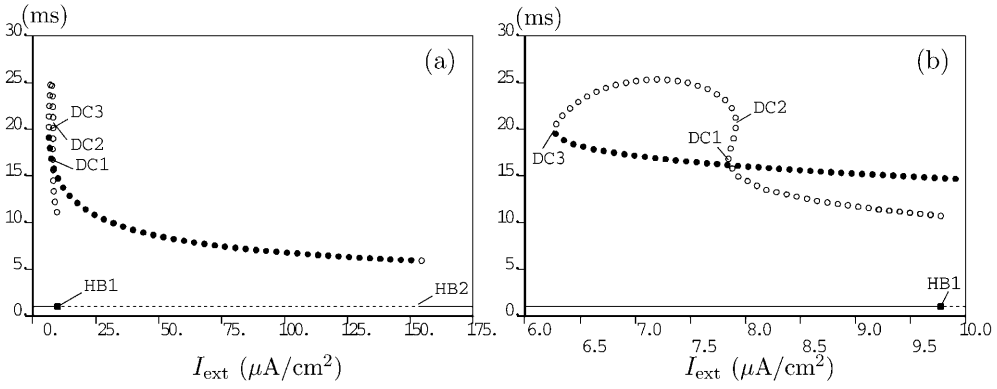

Fig. 5. Period of the periodic solution of the original HH equations

Miller 1980). The fact is that there are more coexisting unstable solutions (data not shown); another period-doubled bifurcated branch may exist at point PD3. Figure 4d shows the membrane potential waveform (only a one-period length of the periodic solution is shown, and the abscissa is the time-normalized by its period) of the unstable periodic solution at point DC1 of Fig. 4c. Figure 4e is the waveform corresponding to the period-doubled solution at point A of Fig. 4c.

We cannot observe these unstable solutions in real experiments. The unstable solutions, however, connect 'the missing links' between stable solutions and help us to understand the total behavior of neuronal models. The bifurcation analysis of Fig. 4 was performed using the computer software package AUTO (Doedel et al. 1995). AUTO can detect several bifurcation points automatically and can trace both stable and unstable branches of equilibria and periodic solutions.

Figure 5a shows the period of the periodic solutions shown in Fig. 4a. Figure 5b is the magnification of Fig. 5a. The period of the stable periodic solutions (closed circle) varies from several to 20 ms. The period does not change much, although the variation is comparatively large in the small I_{ext} range.

Figure 6 shows several one-parameter bifurcation diagrams when the time constant $\bar{\tau}_n$ of the gating variable n is changed. Figure 6a is the case of $\bar{\tau}_n = 100$. The points labeled HB1 and HB2 are again Hopf bifurcation points. At point DC, the double-cycle bifurcation or saddle-node bifurcation of periodic orbits occurs, and a period-doubling bifurcation occurs at point PD. Note that there exist several branches of stable periodic orbits between points DC and PD. However, these branches (such as a period-doubled branch bifurcated from PD) are not shown in this figure for the sake of clarity. On the almost vertical branch bifurcated from HB1, several bifurcations occur and thus we can see switching between closed and open circles. Furthermore, there are many bifurcated branches of periodic orbits between point HB1 and the vertical branch where the membrane potential does not change its waveform but does change its period considerably. These bifurcations are very interesting since they seem to be related to so-called homoclinic bifurcations, but they are very difficult to trace using AUTO. This analysis is now in progress and we will present it elsewhere. The bifurcation diagram of Fig. 6a corresponds to the previous bifurcation diagram of Fig. 3a.

The bifurcation diagram of Fig. 6a-i looks much simpler than Fig. 3a because a maximum value of a periodic solution is plotted in the former while (local) extrema are plotted in the latter. However, if we look at the period we can see such complicated structure again: Fig. 6a-ii shows the periods of periodic orbits of Fig. 6a-i as a function of the bifurcation parameter I_{ext}. In the left region of Fig. 6a-ii, the period changes its value in a very complicated way, and this corresponds to the complicated structure of Fig. 3a. In this region the waveform of the membrane potential is a wide plateau with several sharp spikes superimposed on it plateau (see Fig. 1a–d), while above the I_{ext} values, the membrane potential has a simple waveform with only sharp spikes, although various oscillations are observed between points DC and PD. For example, the waveform of Fig. 1e is a period-doubled solution bifurcated at point PD.

Figure 6b shows the case of $\bar{\tau}_n = 1.5$. This figure is almost the same as that of the original HH equations (see Fig. 4a); the only difference is that the two double-cycle bifurcation points (DC1 and DC2 of Fig. 4) are coalesced (see point Cusp1 in the two parameter bifurcation diagram of Fig. 8a) and disappear as the value of $\bar{\tau}_n$ is slightly increased from $\bar{\tau}_n = 1$. The Hopf bifurcation point HB1 is 'subcritical', and thus unstable periodic orbits are bifurcated here and multi-stability occur, whereas point HB1 of Fig. 6a is 'supercritical'. The stability of the Hopf bifurcation changes between $\bar{\tau}_n = 20$ and $\bar{\tau}_n = 10$ (see point A of Fig. 8a, where the double-cycle bifurcation curve merges with the Hopf bifurcation curve). Figure 6c shows the case in which the value of $\bar{\tau}_n$ is decreased further. In this case, the left Hopf bifurcation point changed its stability again from subcritical to supercritical and thus stable periodic orbits rather than unstable periodic orbits are bifurcated from point HB1.

Figure 7 shows the one-parameter bifurcation diagrams for various values of the time constant $\bar{\tau}_h$ of the gating variable h. Figure 7a is the case of $\bar{\tau}_h = 100$, and corresponds to the bifurcation diagram of Fig. 3b. Figure 7a-ii shows the periods of the periodic orbits rather than their maximum membrane potentials (Fig. 7a-i). These bifurcation diagrams are completely different from the case in which the value of $\bar{\tau}_n$ is changed (Fig. 6) and from the case of the original HH equations (Fig. 4).

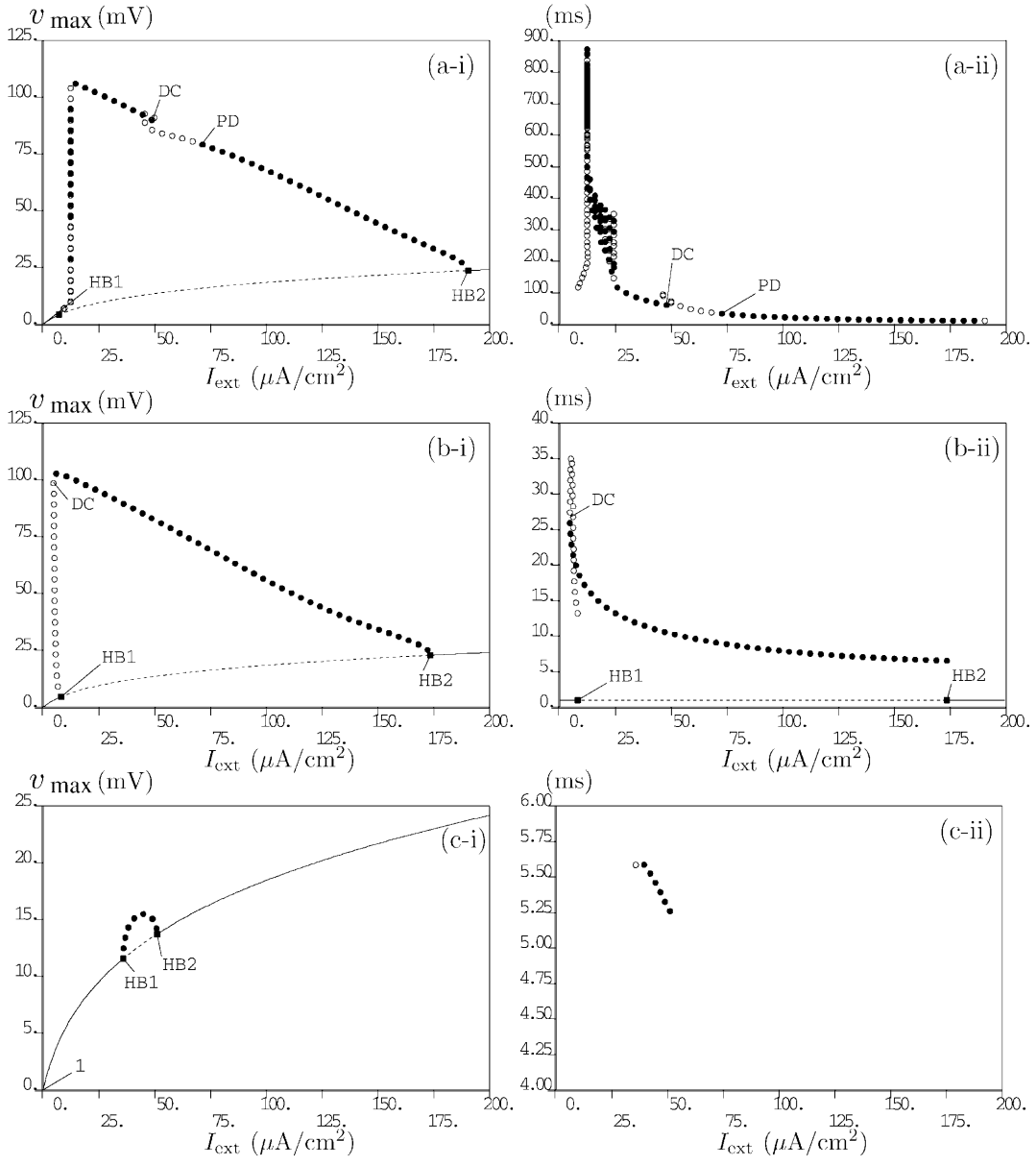

Fig. 6. One-parameter bifurcation diagrams of the HH equations for various values of the time constants $\bar{\tau}_n$: **a** 100, **b** 1.5, and **c** 0.37. *Left column* shows the maximal value of the membrane potential and *right column* shows the period, both as a function of I_{ext}

Points labeled HB1 and HB2 are the sub- and supercritical Hopf bifurcation points, respectively. The stable periodic orbit bifurcated from point HB2 changes its stability at point PD1. At the same time, another stable periodic solution with double period is bifurcated from point PD1. This is the so-called period-doubling bifurcation, in which the period of the bifurcated periodic solution is twice the period of the original periodic solution (see Fig. 7a-ii). The second period-doubling bifurcation occurs at point PD2 on the branch which is bifurcated at point PD1, and the period of the resulting periodic solution is further doubled.

In Fig. 7a it is difficult to distinguish points PD1 and PD2 and apparently there are no stable periodic solutions (closed circle) on the bifurcated branch by the period-doubling bifurcation. However, there is a small region on the bifurcated branch where stable periodic solutions exist, although it is invisible at this scale. Moreover, there are more period-doubling bifurcations near the value of the bifurcation parameter I_{ext}; there is a cascade of period-doubling bifurcations to chaotic solutions (Guckenheimer and Holmes 1983). There are more cascades of period-doubling bifurcations which start at different periodic orbits although we have shown only one cascade of period-doubling bifurcations here for the sake of clarity. Thus we can consider that these cascades of period-doubling bifurcations organize the total response of the HH neuron to external currents and make the response chaotic when h is slow.

Figure 7b shows similar diagrams (cf. Fig. 7a) when the value of $\bar{\tau}_h$ is decreased ($\bar{\tau}_h = 30$) and Fig. 7b-ii shows the corresponding period also. The only difference from the case of $\bar{\tau}_h = 100$ is the two double-cycle bifurcations labeled by DC1 and DC2. These bifurca-

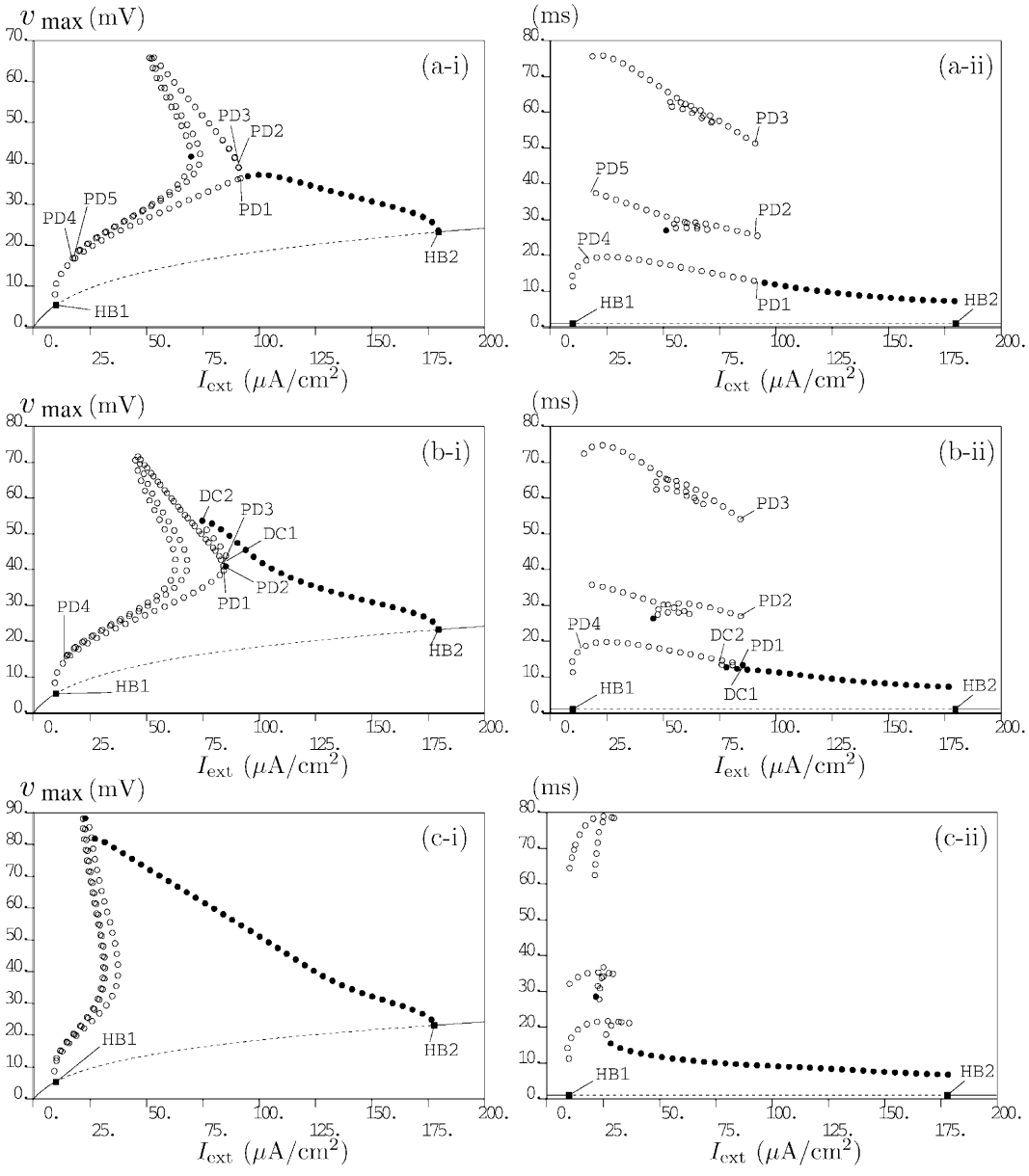

Fig. 7. One-parameter bifurcation diagrams of the HH equations for various values of the time constants $\bar{\tau}_h$: **a** 100, **b** 30, and **c** 5. *Left* and *right columns* show the maximal value of the membrane potential and the period as a function of I_{ext}, respectively

tions are generated at the same time from the more degenerate bifurcation point (point Cusp of Fig. 8c below). As a result of these bifurcations, there is a coexistence of two stable periodic solutions near point DC1 (a closed circle labeled as PD2). Similarly to the case of $\bar{\tau}_h = 100$, a period-doubling bifurcation occurs at point PD1 and the second one occurs at point PD2. Again, there are many period-doubling bifurcations in the left part of Fig. 7b-i, and chaotic responses are seen.

This 'horn-like' bifurcation structure can be observed even in the case of a small time constant $\bar{\tau}_h = 5$ (Fig. 7c), although the region where many period-doubling bifurcations and chaotic responses are seen has been shrunk in the small external current region. In conclusion, as opposed to the *n*-slow case, many cascades of period-doubling bifurcations are seen resulting in many chaotic responses.

2.2 Two-parameter bifurcation analysis

So far, the time constants $\bar{\tau}_n$ and $\bar{\tau}_h$ were fixed to certain values and the bifurcation parameter I_{ext} was continuously changed. In this subsection, the time constants are also changed continuously as another bifurcation parameter. These results are summarized in the two-parameter bifurcation diagram of Fig. 8. Figure 8a shows the loci in the plane of two parameters I_{ext} and $\bar{\tau}_n$, where a specific bifurcation occurs. In Fig. 8c, the parameter $\bar{\tau}_h$ is used instead of $\bar{\tau}_n$.

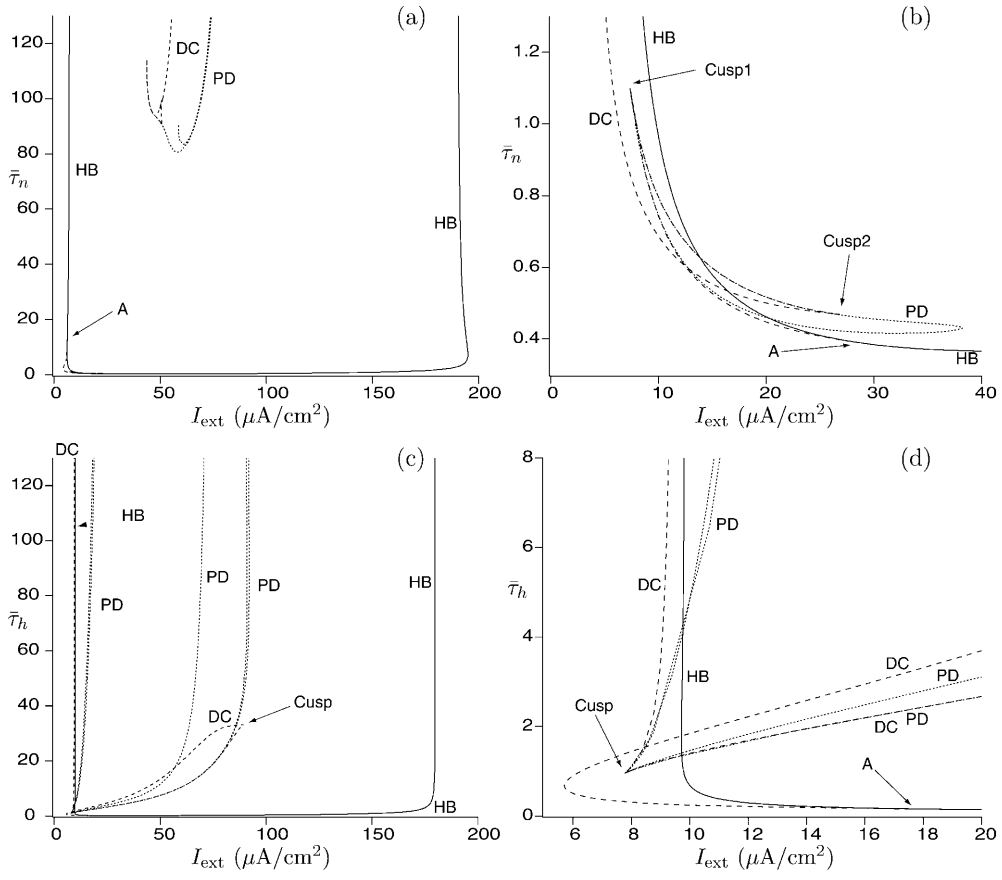

Fig. 8. Two-parameter bifurcation diagram of the HH equations: **a**,**b** *n*-slow case; **c**,**d** *h*-slow case. **b** and **d** are the magnifications of the *lower-left region* of **a** and **c**, respectively. The loci of the Hopf, double-cycle, and period-doubling bifurcations are denoted by *solid*, *broken*, and *dotted lines*, respectively. *Cusp* points are the points where two double-cycle bifurcation curves meet each other, and the point labeled by *A* is the place where a double-cycle bifurcation curve merges with a Hopf bifurcation curve

In Fig. 8b, a horizontal line (not shown) with $\bar{\tau}_n = 1$ corresponds to the one-parameter bifurcation diagram Fig. 4b of the original HH equations. On the line, from the left, we can see three double-cycle bifurcations and Hopf bifurcation in that order (see Fig. 4b). At the leftmost double-cycle bifurcation point, a pair of stable and unstable periodic orbits is generated, and thus the bifurcation relates to the onset of repetitive firings. At the Hopf bifurcation point, the unique equilibrium point changes its stability and unstable periodic orbits are bifurcated. At the point A, a double-cycle bifurcation curve meets with a Hopf bifurcation curve and disappears. The Hopf bifurcation curve changes its 'stability' at the point A; e.g., at points to the left of point A on the Hopf bifurcation curve of Fig. 8b, subcritical Hopf bifurcation occurs while supercritical Hopf bifurcation occurs at points to the right. The cusp points Cusp1 and Cusp2 are the points where two double-cycle bifurcation curves meet and disappear. If we slightly increase the $\bar{\tau}_n$ value above Cusp1, the two double-cycle bifurcation points are not observed in the one-parameter bifurcation diagram (see Fig. 4 and Fig. 6b). So we can say that the parameter set of the original HH equations locates in a very delicate or singular region since slight modification to the parameter values changes the bifurcation structure qualitatively.

Bifurcation points are degenerate or singular points in a certain sense. The cusp points and point A of Fig. 8b at which the Hopf and double-cycle bifurcation curves meet are more singular than the points on all three curves. Such a highly singular point is called an 'organizing center' since several bifurcation curves (less-singular points) gather to the point. Singularity theory (Golubitsky and Schaeffer 1985; Golubitsky et al. 1988) is useful in the analysis of such a complicated bifurcation structure and has been applied to the analysis of HH-type equations (Labouriau 1985, 1989; Hassard and Shiau 1989; Shiau and Hassard 1991; Labouriau and Ruas 1996; Fukai et al. 2000b).

From Fig. 8a,c we can see that the two (left and right) Hopf bifurcation points do not depend much on the time constants $\bar{\tau}_n$ and $\bar{\tau}_h$ (note that the time constants do not affect the position of equilibrium but they do affect its overall stability). In the *h*-slow case (Fig. 8c), several period-doubling curves exist over a wide range of $\bar{\tau}_h$ values. Right-most period-doubling bifurcation curves correspond to stable periodic orbits, while left ones correspond to unstable orbits. There are a cascade of many curves (only one or two are shown) near each period-doubling bifurcation curve and these curves organize many chaotic oscillations in the *h*-slow case (see Fig. 3b). In the following sections, we clarify the reason why the HH response to a constant current is so different in the *n*-slow and *h*-slow cases.

3 Slow–fast decomposition analysis

A system with multiple time scales may be denoted as follows:

$$\frac{dx}{dt} = f(x,y), \quad x \in R^n, \ y \in R^m \tag{2a}$$

$$\frac{dy}{dt} = \epsilon g(x,y), \quad \epsilon \ll 1 \tag{2b}$$

Equation (2b) is called a slow subsystem since the value of y changes slowly, whereas (2a) is a fast subsystem. The whole (2) is called a full system. So-called slow–fast analysis (Rinzel and Lee 1986) divides the full system into the slow and fast subsystems. In the fast subsystem (2a), the slow variable y is considered to be a constant or a parameter. The variable x changes more quickly than y, and thus x is considered to stay close to the attractor (e.g., stable equilibrium point or limit cycle) of the fast subsystem for a fixed value of y. The variable y changes slowly with a velocity $\epsilon g(x,y)$, in which x is considered to be in the attractor. The attractor of the fast subsystem may change if y is varied. The problem of analysis of the dependency of the attractor on the parameter y is a bifurcation problem. Thus the slow–fast analysis reduces the analysis of the full system to the bifurcation problem of the fast subsystem with a slowly-varying bifurcation parameter.

In the case that the gating variable $n(h)$ of the HH equations (1) is slow, the corresponding slow subsystem is (1c) (Eq. 1d) and the remaining equations (1a, b, d) (Eqs. 1a, b, c, resp.) are the fast subsystem.

3.1 The n-slow case

Figure 9a shows the waveforms of membrane potential v and gating variable n when n is slow. The action potential is sharp, followed by a wide 'plateau' similar to an action potential of heart muscle cells, and the gating variable varies slowly.

Figure 9b is the bifurcation diagram of the fast subsystem (1a, b, d) in which n is considered a bifurcation parameter. The Z-shaped curve denotes the equilibrium point of the fast subsystem as a function of n. At the point labeled SN1 or SN2, a saddle-node bifurcation of equilibria occurs and a pair of equilibria appears or disappears. At point HB, a subcritical Hopf bifurcation occurs, and the stability of equilibria changes resulting in unstable periodic orbits bifurcating from the equilibrium.

Next we take the motion of the slow variable n into account. Figure 9c shows the superposition of the projection of the solution of the full system (1) to n–v phase plane on the bifurcation diagram of the fast subsystem. Let us start at the point labeled A. At this point, the solution orbit of the full system stays near a stable equilibrium of the fast subsystem (lower branch of the Z-shaped curve). The almost straight line labeled

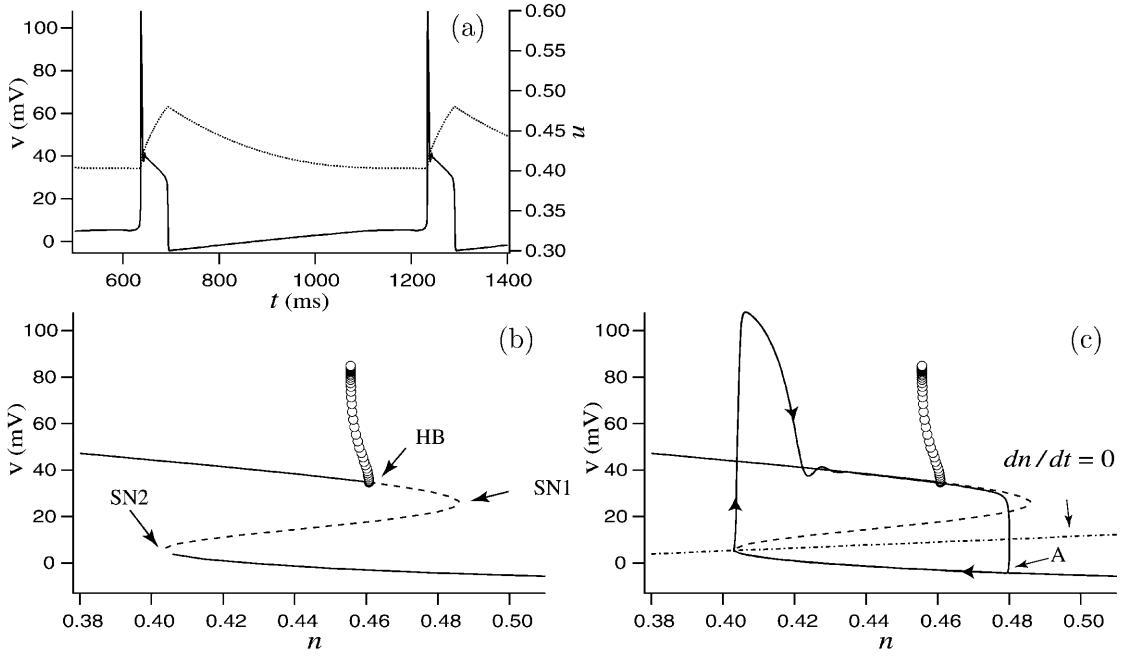

Fig. 9. **a** Waveforms of membrane potential v (*solid line*) and gating variable n (*dotted line*) when n is slow ($\bar{\tau}_n = 100$, $I_{ext} = 10$). **b** Bifurcation diagram of the fast subsystem. **c** Superposition of the orbit (*closed curve with arrows*) of the full system in **b**. The Z-shaped curves of **b** and **c** denote the equilibria of the fast subsystem ($dv/dt = dm/dt = dh/dt = 0$) as a function of the slow variable n (*solid line* denotes a stable equilibrium and *dashed line* an unstable one; the *open circles* denote unstable periodic orbits). The almost straight curve labeled by $dn/dt = 0$ is the n-nullcline and denotes the equilibria of the slow subsystem as a function of n. *SN1* and *SN2* are the saddle-node bifurcation points

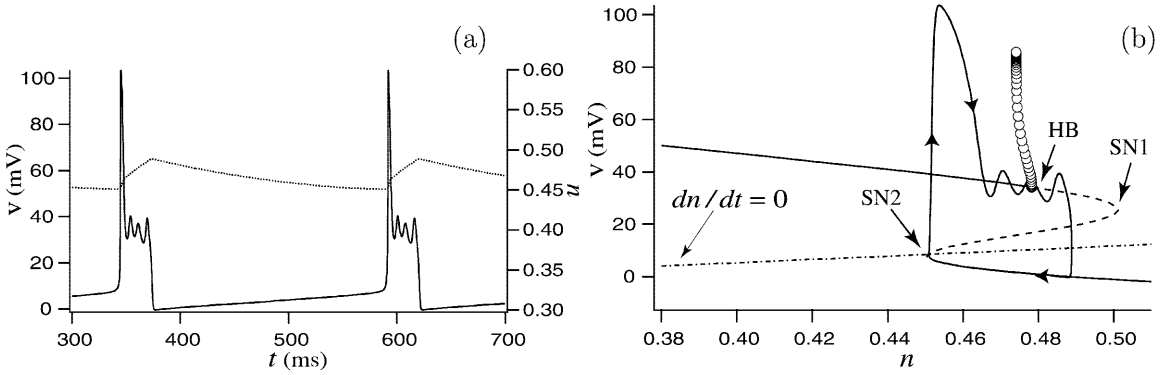

Fig. 10. **a** Waveforms of membrane potential v (*solid line*) and gating variable n (*dotted line*) when n is slow ($\bar{\tau}_n = 100$, $I_{\text{ext}} = 20$). **b** Superposition of the orbit (*closed curve with arrows*) of the full system on the bifurcation diagram of the fast subsystem

$\mathrm{d}n/\mathrm{d}t = 0$ is the n-nullcline. Since the point A is below this curve, and thus $\mathrm{d}n/\mathrm{d}t < 0$, the orbit of the full system moves slowly to the left of A following the lower branch. When n decreases to close to 0.4, the stable equilibrium point of the fast subsystem disappears by the saddle-node bifurcation SN2, and thus the orbit of the full system quickly jumps to the upper branch. Then, since the inactivation process (h) is relatively slow and so some time is needed before the orbit of the full system approaches the upper branch, a sharp spike appears in the membrane waveform of Fig. 9a.

On the upper branch $\mathrm{d}n/\mathrm{d}t > 0$, and thus the orbit moves rightwards slowly. If the orbit passes through the Hopf bifurcation HB, the orbit cannot stay near the upper branch since the equilibrium of the fast subsystem becomes unstable. Then the orbit jumps to the lower branch and repeats the above process. Note that the jump point on the upper branch is not close to the point HB. Such a delay of the departure at the slow passage of a Hopf bifurcation occurs in the general situation (Neishtadt 1987, 1988; Baer et al. 1989; Mandel and Erneux 1989).

Figure 10a shows the membrane potential waveform when $I_{\text{ext}} = 20$. Comparing this figure with Fig. 9a, as the value of I_{ext} changes from 10 to 20, the total period of the oscillation becomes one-third, and an oscillatory wave in the plateau region appears (there are also small oscillations in the plateau region in Fig. 9a). We now consider why such a slight increase in the value of I_{ext} changes the characteristics of total oscillations so much. Figure 10b shows the superposition of the bifurcation diagram of the fast subsystem and the orbit of the full system, similar to Fig. 9c. Differently from the case of $I_{\text{ext}} = 10$, the bifurcation point SN2 moves significantly to the right and SN1 moves only slightly, and thus the distance between SN1 and SN2 is less. Since the orbit of the full system spends much time on the upper or lower branch between SN1 and SN2, as the distance between SN1 and SN2 decreases, the total period of the oscillation as decreases. The distance between SN2 and the Hopf bifurcation point HB is also reduced. As a result, the attraction of the orbit of the full system at SN2 to the upper branch is weakened, and thus a big oscillation appears in the plateau region.

The reason why an increase in the value of I_{ext} decreases the distance between SN1 and SN2 is as follows. The value of membrane potential v of the equilibria of the fast subsystem is obtained by

$$\begin{aligned} &G(v, m^{\infty}(v), n, h^{\infty}(v)) + I_{\text{ext}} \\ &\quad = \bar{g}_{\text{Na}}(m^{\infty}(v))^3 h^{\infty}(v)(V_{\text{Na}} - v) + \bar{g}_{\text{K}} n^4 (V_{\text{K}} - v) \\ &\qquad + \bar{g}_{\text{L}}(V_{\text{L}} - v) + I_{\text{ext}} = 0 \end{aligned} \tag{3}$$

Solving this equation for n, we obtain

$$n^4 = \frac{\bar{g}_{\text{Na}}(m^{\infty}(v))^3 h^{\infty}(v)(V_{\text{Na}} - v) + \bar{g}_{\text{L}}(V_{\text{L}} - v) + I_{\text{ext}}}{\bar{g}_{\text{K}}(v - V_{\text{K}})} \tag{4}$$

The Z-shaped curves of Figs. 9b and 10b were plotted using the relation between v and n determined by (4). Since both denominator and numerator of the right-hand side of (4) are positive, the increase in the value of I_{ext} increases n. This means that the increase of I_{ext} moves the Z-shaped curves to the right. The amount of displacement becomes bigger if the value of v is decreased, since the value of the denominator $\bar{g}_{\text{K}}(v - V_{\text{K}})$ of (4) decreases as v decreases. Thus, the lower part of the curves is displaced more than the upper part. This is why the Z-shaped curves shrinks as I_{ext} is increased.

Figure 11 shows the case of $I_{\text{ext}} = 50$. There are no plateau regions in the membrane potential waveform and the waveform resembles the nervous impulse of the original (no time-scale change) HH equations. However, the period of this repetitive firing is much longer than that of the original HH equations since the state point spends more time on the lower branch. As is seen from Fig. 11b, the increase in I_{ext} further shrinks the distance between SN1 and SN2, and the Hopf bifurcation point comes to the left of SN2. Thus the orbit of the full system that jumps from the lower branch of the Z-shaped curve does not approach the upper branch (since the upper branch is unstable), but it does approach the stable periodic orbit of the fast subsystem (denoted by closed circles) before returning to the lower branch after it generates one spike. In Fig. 11, unstable periodic

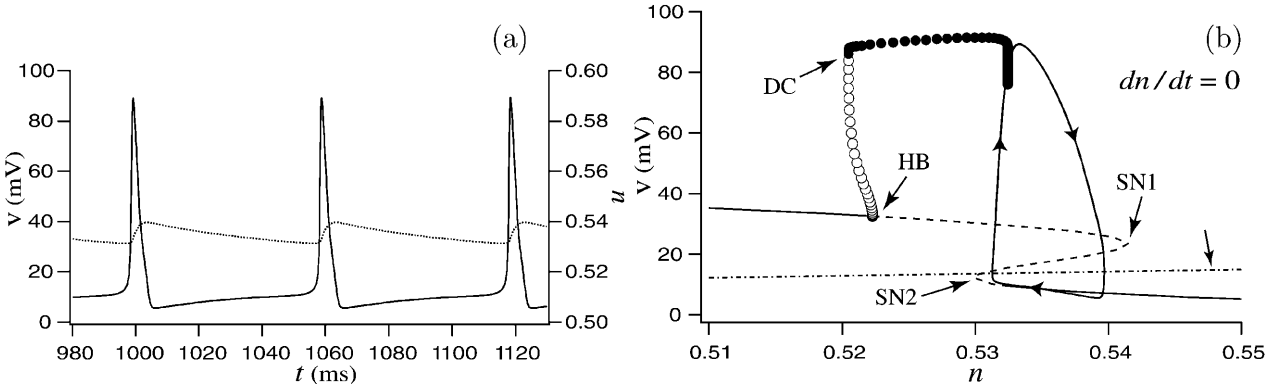

Fig. 11. **a** Waveforms of membrane potential v (*solid line*) and gating variable n (*dotted line*) when n is slow ($\bar{\tau}_n = 100$, $I_{\text{ext}} = 50$). **b** Superposition of the orbit (*closed curve with arrows*) of the full system on the bifurcation diagram of the fast subsystem

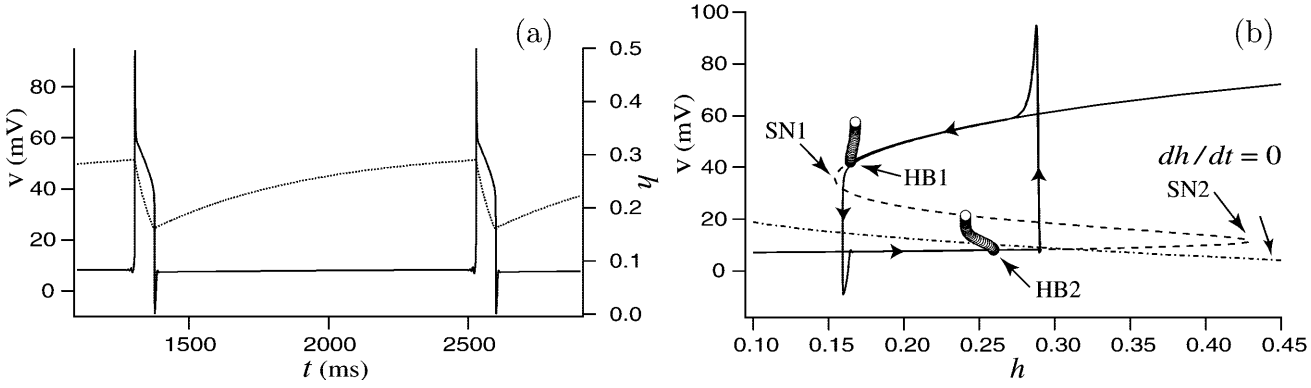

Fig. 12. **a** Waveforms of membrane potential v (*solid line*) and gating variable h (*dotted line*) when h is slow ($\bar{\tau}_h = 100$, $I_{\text{ext}} = 20$). **b** Superposition of the orbit (*closed curve with arrows*) of the full system on the bifurcation diagram of the fast subsystem. The S-shaped curve denotes the equilibria of the fast subsystem ($\mathrm{d}v/\mathrm{d}t = \mathrm{d}m/\mathrm{d}t = \mathrm{d}n/\mathrm{d}t = 0$) as a function of the slow variable h. The almost straight curve labeled by $\mathrm{d}h/\mathrm{d}t = 0$ is the h-nullcline and denotes the equilibria of the slow subsystem as a function of h

orbits of the fast subsystem branched from the Hopf bifurcation point HB change their stability by the double cycle bifurcation labeled by DC, and suddenly terminate around $n = 0.533$ by the homoclinic bifurcation (of the fast subsystem).

3.2 The h-slow case

Next we consider the case of h-slow ($\bar{\tau}_h = 100$). Figure 12a shows the waveforms of membrane potential v and gating variable h when h is slow. The membrane potential has a wide plateau similar to the case of n-slow. The only difference from the n-slow case is that the membrane potential of the h-slow case has a sharp (downward) spike in the hyperpolarized region ($v < 0$) beside the depolarized region. Figure 12b is the bifurcation diagram of the fast subsystem (1a, b, c) in which h is considered as a bifurcation parameter and the orbit of the full system is also superimposed. The S-shaped curve denotes the equilibria of the fast subsystem as a function of the slow variable h obtained by:

$$h = \frac{\bar{g}_{\text{K}}(n^{\infty}(v))^4(V_{\text{K}} - v) + \bar{g}_{\text{L}}(V_{\text{L}} - v) + I_{\text{ext}}}{\bar{g}_{\text{Na}}(m^{\infty}(v))^3(v - V_{\text{Na}})} \tag{5}$$

Similarly to the n-slow case, the orbit of the full system moves alternately on the upper and lower branches of the S-shaped curve. Differently from the n-slow case, the orbit moves rightward below the h-nullcline ($\mathrm{d}h/\mathrm{d}t = 0$) and leftward above it. This is because h is an inactivation variable while n is an activation one; $h^{\infty}(v)$ is a decreasing function of v while $n^{\infty}(v)$ is an increasing function. As is seen from Fig. 12b, both switchings between upper and lower branches are caused by the Hopf bifurcations (HB1 and HB2). We note that the orbit does not leave the branch right at the bifurcation points, but there are some delays as stated above.

Let us compare Fig. 12b with the n-slow cases (Figs. 9b, 10b, and 11b). There seems to be no essential difference between the dynamics of n-slow and h-slow cases except that the bifurcation diagrams of the fast subsystem are mirror images. The n-nullcline intersects the Z-shaped curve in the middle branch whereas the h-nullcline intersects the S-like curve in the lower branch. This leads to a big difference between n- and h-slow cases.

Figure 13a shows the membrane potential waveform when h is slow and $I_{\text{ext}} = 50$. The waveform is very different from those shown before. This is a (type III) chaotic bursting oscillation in which an active phase with several spikes and a silent phase with no spikes

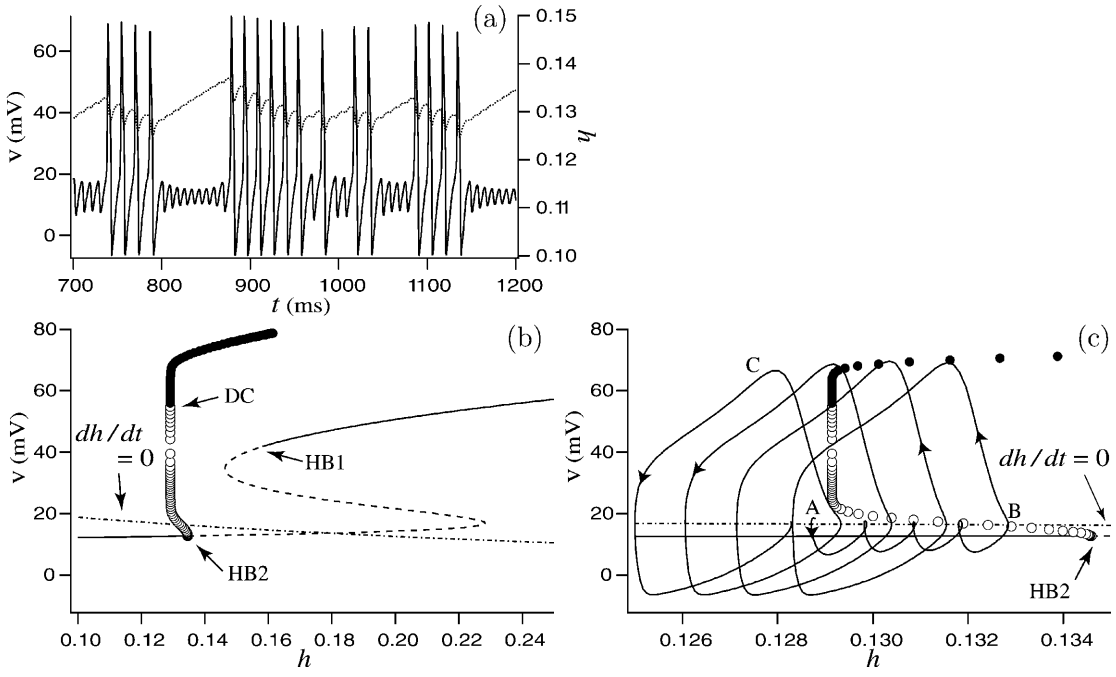

Fig. 13. **a** Waveforms of membrane potential v (*solid line*) and gating variable h (*dotted line*) when h is slow ($\bar{\tau}_h = 100$, $I_{\text{ext}} = 50$). **b** Bifurcation diagram of the fast subsystem. **c** Superposition of the orbit (*solid curve with arrows*) of the full system on **b**

appear alternately, and the number of spikes in the active phase varies chaotically cycle-by-cycle. (See Bertram et al. 1995; Wang and Rinzel 1995; Hoppensteadt and Izhikevich 1997 for the topological classification of bursting oscillations.) Figure 13b is the bifurcation diagram of the fast subsystem. Comparing with Fig. 10b, the S-shaped curve shrinks and moves leftward by the increase of the value of I_{ext}. As a result, the Hopf bifurcation point HB2 moves leftward and the periodic orbits that bifurcate from HB2 change their stability at the double-cycle bifurcation point DC. In the range of $0.130 < h < 0.135$, stable equilibria coexist with stable periodic orbits (bistability).

Figure 13c is the superposition of the orbit of full system (the first 100 ms of Fig. 13a is drawn) on the magnification of the fast-bifurcation diagram of Fig. 13b. The orbit started at point A moves rightwards since the lower branch of the S-shaped curve is below the h-nullcline $\mathrm{d}h/\mathrm{d}t = 0$. The orbit of the full system crosses the unstable periodic orbit of the fast subsystem at point B, then the orbit changes its direction to the stable periodic orbit of the fast subsystem. When the orbit of full system stays near the periodic orbit of the fast subsystem, the value of h decreases since the membrane potential of the periodic orbit is above the h-nullcline 'on average'. After several spikes are generated, the orbit leaves the stable periodic orbit of the fast subsystem at point C and returns to a stable equilibrium. This return point is not same as the starting point A, and thus chaotic oscillation may appear. The exact generation mechanism of this chaotic (bursting) oscillation has not yet been characterized well. However, we give a very rough picture about this mechanism as follows: As stated above, the silent phase of the bursting oscillation ends and an active phase starts when the orbit of the full system crosses an unstable periodic orbit of the fast subsystem whose maximum value is denoted by an open circle. This crossing time is very sensitive to the timing of the beginning of the silent phase, since the stability of the equilibrium points of the fast subsystem (lower branch) is weak and the orbit of the full system winds the equilibria. This sensitivity seems to lead to the so-called 'sensitive dependence on initial conditions' of chaos. Thus, we conjecture that type-III burstings using Bertram's terminology (Bertram et al. 1995: the active phase begins at a subcritical Hopf bifurcation point and ends at a double-cycle bifurcation point of the fast subsystem) have great relevance to the generation of chaotic bursting oscillation.

When h is slow – over a wide range of the values of I_{ext} – the structure of the bifurcation diagram of the fast subsystem is similar to that of Fig. 13b. Therefore, chaotic bursting oscillations like those in Fig. 13a are observed over a wide range of I_{ext} values. Thus, the response characteristics (Fig. 3) of the modified HH equations to a constant current are quite different between n-slow and h-slow cases.

4 Generation and annihilation of chaotic oscillation

As is seen above, the only topological or qualitative difference between n- and h-slow cases is that in the n-slow case, the Z-shaped equilibrium curve of the fast subsystem intersected the n-nullcline (the equilibrium curve of the slow subsystem) in the middle branch, whereas in the h-slow case the intersection was in the lower branch of the S-shaped curve. From this obser-

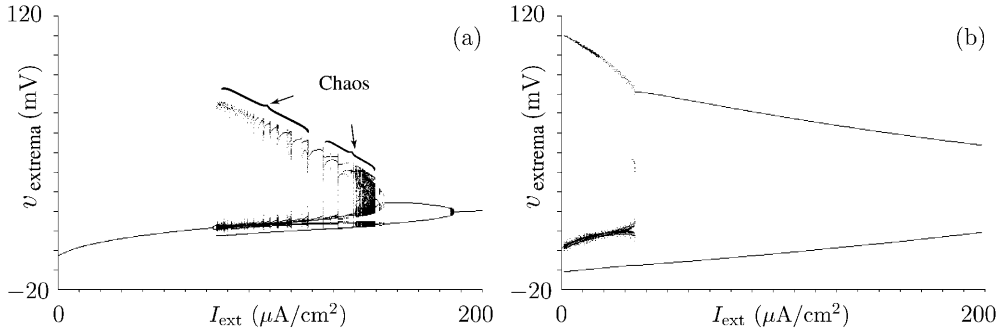

Fig. 14a,b. Bifurcation diagram of the HH equations (1) with voltage shifts for the external constant current I_{ext}. Local extrema of membrane potential $v(t)$ are plotted for each value of I_{ext}. **a** The n-slow case ($\bar{\tau}_n = 100$, $\bar{\tau}_m = \bar{\tau}_h = 1$). **b** The h-slow case ($\bar{\tau}_h = 100$, $\bar{\tau}_m = \bar{\tau}_n = 1$)

vation, we suspect that the method of intersection of two equilibria curves of the fast subsystem and of slow subsystem differentiates the response characteristics of the HH equations to a constant current between n-slow (Fig. 3a) and h-slow cases (Fig. 3b). In order to verify this conjecture, we alter the method of intersection of the equilibria curves of the fast subsystem and slow subsystem. To do so, we have shifted the functions $n^\infty(v)$ and $h^\infty(v)$ to $n^\infty(v+5)$ and $h^\infty(v-10)$, respectively. Then the intersections occur in the lower branch in the n-slow case and in the middle branch in the h-slow case. Figure 14a (Fig. 14b) shows the response characteristics of the n-slow (h-slow) HH equations with $n^\infty(v)$ ($h^\infty(v)$, resp.) shifted in this way. Figure 14a becomes considerably different from Fig. 3a to rather resemble Fig. 3b, and various chaotic responses are seen in Fig. 14a while almost all chaotic responses of Fig. 3b are annihilated in Fig. 14b. From this observation, we conclude that the topological feature of the intersection of the equilibria curves of slow and fast subsystems is the most important factor in the global response characteristics of the neuronal model.

5 Discussion

We have proposed the modified Hodgkin–Huxley equations (1) as a prototypical neuron model with the simplest formulation and exhibiting a variety of dynamics. In fact, the equations could produce various kinds of membrane waveforms that are observed in diverse neurons. If a parameter such as the potassium equilibrium potential V_K of the original HH equations in addition to the I_{ext} value is changed, various complicated phenomena appear (Guckenheimer and Labouriau 1993; Fukai et al. 2000a). The V_K value changes the *number* and stability of equilibrium points, and this change makes the bifurcation analysis very complicated. Our modified HH equations, however, have an advantage that the change of time constants changes only the stability of the unique equilibrium point of the original HH equations and does not change the number of equilibria. Thus the modified HH equations represent a good typical model from the diverse family of HH-type equations.

Using the slow–fast analysis, we have shown that the topological feature of the intersection of the equilibrium curves of fast and slow subsystems determines the behavior of the full system. We emphasize that the topological character of equilibria do not have much relevance to the oscillatory behavior of the system in general. In our system, however, we can predict oscillatory (chaotic) behavior from the simple nature of equilibria curves.

The (modified) HH equations with large time constants are mathematically a singularly perturbed system. In such systems, if a slow variable passes through a bifurcation point of the fast subsystem, then unexpected phenomena such as the delay at a Hopf bifurcation point (Neishtadt 1987, 1988; Baer et al. 1989; Mandel and Erneux 1989) would be observed. However, many phenomena have not yet been clarified mathematically (Guckenheimer 1996) in spite of the long history of research into the singular perturbation method.

In the slow–fast analysis used in this article, the number of slow variables was unity. Such slow–fast analysis is also applicable to the case of more slow variables; in fact, the bursting β-cell model with two slow variables has been analyzed already (Smolen et al. 1993). We note that if both variables n and h are slow in the modified HH equations, then the dynamics is not so interesting; it is very similar to that of the original HH equations. Thus, the time-scale difference between n and h is essential in the modified HH equations.

We have shown numerically that chaotic oscillations appear everywhere when the slow variable passes a double-cycle bifurcation point and a subcritical Hopf bifurcation point of a fast subsystem, which leads to a so-called type III bursting oscillation (Bertram et al. 1995). For a rigorous mathematical analysis, more elaborate use of the geometric singular perturbation method (Jones and Kopell 1994) would be useful. For a chaotic oscillation when a slow variable passes a homoclinic bifurcation of a fast subsystem, see Terman (1991).

Acknowledgments. This research was partially supported by the Japanese Ministry of Education, Science, Sports and Culture, Grant-in-Aid (#10650429). We thank the anonymous referees for their many valuable suggestions for improving the original manuscript.

References

Alexander JC, Cai DY (1991) On the dynamics of bursting systems. J Math Biol 29: 405–423

Av-Ron E (1994) The role of a transient potassium current in a bursting neuron model. J Math Biol 33: 71–87

Baer SM, Erneux T, Rinzel J (1989) The slow passage through a Hopf bifurcation: delay, memory effects, and resonance. SIAM J Appl Math 49: 55–71

Bedrov YA, Akoev GN, Dick OE (1992) Partition of the Hodgkin–Huxley type model parameter space into the regions of qualitatively different solutions. Biol Cybern 66: 413–418

Bertram R (1994) Reduced-system analysis of the effects of serotonin on a molluscan burster neuron. Biol Cybern 70: 359–368

Bertram R, Butte MJ, Kiemel T, Sherman A (1995) Topological and phenomenological classification of bursting oscillations. Bull Math Biol 57: 413–439

Canavier CC, Clark JW, Byrne JH (1991) Simulation of the bursting activity of neuron R15 in *Aplisia*: role of ionic currents, calcium balance, and modulatory transmitters. J Neurophysiol 66: 2107–2124

Canavier CC, Baxter DA, Clark JW, Byrne JH (1993) Nonlinear dynamics in a model neuron provide a novel mechanism for transient synaptic inputs to produce long-term alterations of postsynaptic activity. J Neurophysiol 69: 2252–2257

Chay TR, Keizer J (1983) Minimal model for membrane oscillations in the pancreatic β-cell. Biophys J 42: 181–190

Chay TR, Rinzel J (1985) Bursting, beating, and chaos in an excitable membrane model. Biophys J 47: 357–366

Clay JR (1998) Excitability of the squid giant axon revisited. J Neurophysiol 80: 903–913

Cronin J (1987) Mathematical aspects of Hodgkin–Huxley neural theory. Cambridge University Press, Cambridge

Doedel E, Wang X, Fairgrieve T (1995) AUTO94 – Software for continuation and bifurcation problems in ordinary differential equations. CRPC-95-2, California Institute of Technology

Doi S, Sato S (1995) The global bifurcation structure of the BVP neuronal model driven by periodic pulse trains. Math Biosci 125: 229–250

Doi S, Inoue J, Sato S, Smith CE (1999) Bifurcation analysis of neuronal excitability and oscillations. In: Poznanski R (ed) Modeling in the neurosciences: from ionic channels to neural networks. Harwood Academic Reading, pp 443–473

Fukai H, Doi S, Nomura T, Sato S (2000a) Hopf bifurcations in multiple parameter space of the Hodgkin–Huxley equations. I. Global organization of bistable periodic solutions. Biol Cybern 82: 215–222

Fukai H, Nomura T, Doi S, Sato S (2000b) Hopf bifurcations in multiple parameter space of the Hodgkin–Huxley equations. II. Singularity theoretic approach and highly degenerate bifurcations. Biol Cybern 82: 223–229

Golubitsky M, Schaeffer D (1985) Singularities and groups in bifurcation theory I. Springer, Berlin Heidelberg New York

Golubitsky M, Stewart I, Schaeffer D (1988) Singularities and groups in bifurcation theory II. Springer, Berlin Heidelberg New York

Guckenheimer J (1996) Towards a global theory of singularly perturbed dynamical systems. Prog Nonlinear Differ Equations Appl 19: 213–225

Guckenheimer J, Holmes P (1983) Nonlinear oscillations, dynamical systems, and bifurcation of vector fields. Springer, Berlin Heidelberg New York

Guckenheimer J, Labouriau IS (1993) Bifurcation of the Hodgkin and Huxley equations: A new twist. Bull Math Biol 55: 937–952

Guttman R, Lewis S, Rinzel J (1980) Control of repetitive firing in squid axon membrane as a model for neuroneoscillator. J Physiol 305: 377–395

Hassard B (1978) Bifurcation of periodic solutions of the Hodgkin–Huxley model for the squid giant axon. J Theor Biol 71: 401–420

Hassard BD, Shiau LJ (1989) Isolated periodic solutions of the Hodgkin–Huxley equations. J Theor Biol 136: 267–280

Hille B (1992) Ionic channels of excitable membranes, 2nd edn. Sinauer Associates, Sunderland, Mass.

Hodgkin AL, Huxley AF (1952) A quantitative description of membrane current and its applications to conduction and excitation in nerve. J Physiol 117: 500–544

Hoppensteadt FC, Izhikevich EM (1997) Weakly connected neural networks. Springer, Berlin Heidelberg New York

Jones C, Kopell N (1994) Tracking invariant manifolds with differential forms. J Diff Eq 108: 64–88

Keener J, Sneyd J (1998) Mathematical physiology. Springer, Berlin Heidelberg New York

Labouriau IS (1985) Degenerate Hopf bifurcation and nerve impulse. SIAM J Math Anal 16: 1121–1133

Labouriau IS (1989) Degenerate Hopf bifurcation and nerve impulse. Part II. SIAM J Math Anal 20: 1–12

Labouriau IS, Ruas MAS (1996) Singularities of equations of Hodgkin–Huxley type. Dyn Stab Syst 11: 91–108

Mandel P, Erneux T (1989) The slow passage through a steady bifurcation: delay and memory effects. J Stat Phys 48: 1059–1070

Neishtadt AI (1987) Persistence of stability loss for dynamical bifurcations I. Differ Equations 23: 1385–1391

Neishtadt AI (1988) Persistence of stability loss for dynamical bifurcations II. Differ Equations 24: 171–176

Noble D (1995) The development of mathematical models of the heart. Chaos Solitons Fractals 5: 321–333

Plant RE (1976) The geometry of the Hodgkin–Huxley model. Comp Prog Biomed 6: 85–91

Rinzel J (1978) On repetitive activity in nerve. Fed Proc 37: 2793–2802

Rinzel J (1990) Electrical excitability of cells, theory and experiment: review of the Hodgkin–Huxley foundation and update. Bull Math Biol 52: 5–23

Rinzel J, Lee YS (1986) On different mechanisms of membrane potential bursting. In: Othmer HG (ed) Nonlinear oscillations in biology and chemistry. Springer, Berlin Heidelberg New York, pp 19–33

Rinzel J, Miller RN (1980) Numerical calculation of stable and unstable periodic solutions to the Hodgkin–Huxley equations. Math Biosci 49: 27–59

Rush ME, Rinzel J (1995) The potassium A-current, low firing rates and rebound excitation in Hodgkin–Huxley models. Bull Math Biol 57: 899–929

Schweighofer N, Doya K, Kawato M (1999) Electrophysiological properties of inferior olive neurons: a compartmental model. J Neurophysiol 82: 804–817

Shiau LJ, Hassard BD (1991) Degenerate Hopf bifurcation and isolated periodic solutions of the Hodgkin–Huxley model with varying sodium ion concentration. J Theor Biol 148: 157–173

Smolen P, Terman D, Rinzel J (1993) Properties of a bursting model with two slow inhibitory variables. SIAM J Appl Math 53: 861–892

Strassberg AF, DeFelice LJ (1993) Limitations of the Hodgkin–Huxley formalism: effects of single channel kinetics upon transmembrane voltage dynamics. Neural Comput 5: 843–855

Terman D (1991) Chaotic spikes arising from a model of bursting in excitable membranes. SIAM J Appl Math 51: 1418–1450

Traub RD, Wong RKS, Miles R, Michelson H (1991) A model of a CA3 hippocampal pyramidal neuron incorporating voltage-clamp data on intrinsic conductances. J Neurophysiol 66: 635–650

Troy WC (1978) The bifurcation of periodic solutions in the Hodgkin–Huxley equations. Q Appl Math 36: 73–83

Wang XJ, Rinzel J (1995) Oscillatory and bursting properties of neurons. In: Arbib MA (ed) The handbook of brain theory and neural networks. MIT Press, pp 686–691